Molecular Determinants for Binding of Ammonium Ion in the Ammonia Transporter AmtB—A Quantum Chemical Analysis†

Yuemin Liu and Xiche Hu*

Department of Chemistry, University of Toledo, Toledo, Ohio 43606

Received: August 1, 2005; In Final Form: October 27, 2005

The transport of ammonium across the cell membrane represents an important biological process in all living organisms. The mechanisms for ammonium translocation were analyzed by computer simulations based on first principles. Intermolecular interaction energies between the differentially methylated ammonium and the ammonium channel protein AmtB were calculated by means of the supermolecular approach at the MP2/6-311+G* level based on the high-resolution crystal structures of ligand-bound protein complexes. Our analysis attributes the molecular determinants for protein−ligand recognition in ammonium transporter AmtB to the aromatic cage formed by three aromatic residues Phe103, Phe107, and Trp148, as well as Ser219. The former residues are involved in cation−π interactions with the positively charged methylated ammoniums. The latter residue acts as a hydrogen bond acceptor to ammonium. Thus, this work provides directly the missing evidence for the hypothesized role played by the wider vestibule site of AmtB at the periplasmic side of the membrane in "recruiting" NH_4^+ or methylammonium ions as proposed by Khademi et al. (*Science* **2004**, *305*, 1587). In addition, a hybrid quantum mechanics/molecular mechanics scheme was applied to optimize the structures of differentially methylated ammoniums in the AmtB protein, which generated structural and energetic data that provide a satisfactory explanation to the experimental observation that tetramethylammonium is not inhibitory to conducting ammonium and methylammonium in the ammonium transport channel.

I. Introduction

The transport of ammonium (Am) across cell membranes represents one of the fundamental processes in microorganisms, plants, animals, and humans. The distribution of Am transporter proteins [Am transporter/methylammonium (MA) permeases/rhesus, commonly abbreviated as Amt/MEP/Rh] indicates that the process of Am transport has been conserved throughout evolution.[1,2] Microorganisms and plants use Am as the primary source of inorganic nitrogen.[2−5] For animals and humans, sequestration and excretion of cytotoxic Am serve as parts of the liver and kidney physiology.[6−8] The Am ion NH_4^+ is a neurotoxin and must be efficiently cleared from the portal blood by hepatocytes. When Am ion concentrations elevate, advanced liver failure, as seen in hepatic encephalopathy, can result in dysfunction of the central nervous system. It is known that many kinds of neurological disorders, from seizures to stupor and coma, result from overexposure to ammonia.

Ammonia (NH_3) is a gas, but when dissolved in water, it exists predominantly as the Am ion (NH_4^+) with a pK_a of 9.25 in biological fluids. The means by which Am enters cells were not clear until genes encoding high-affinity Amts were isolated.[3,9] It is now known that Amt is a transport protein present in the bacterial inner membrane between the cytoplasmic and the periplasmic spaces that facilitates NH_3 uptake. They have also been found to be involved in cellular responses to Am availability in organisms. The human counterpart Rh proteins [Rh-associated glycoprotein (RhAG), RhCE, and RhD] act as an important kind of blood group antigens in the membranes of red blood cells. Nonerythroid Rh proteins (RhBG and RhCG) serve as Amts in the liver and kidney, which are coupled to Am metabolism.[10,11]

In general, transporter proteins in biological membranes can be categorized into channels and carriers depending on their extent of flexibility and mobility in translocating substrates. Channels work as selective pores that open in response to an external stimulus, enabling movement of a solute down an electrochemical gradient. Active carrier proteins use an energy-producing process to translocate a substrate against a concentration gradient. Amt belongs to the conducting channel rather than carrier. Like most channel proteins, it mainly consists of 11 membrane-spanning α-helices with the N terminus on the exterior face of the membrane and the C terminus on the interior.[4]

Recently, high-resolution crystal structures of Am channel protein AmtB from *Escherichia coli*, as a representative channel protein of the Amt/MEP/Rh family, have been determined by X-ray crystallography.[12,14] Overall, the structures reveal the channel's three identical membrane-spanning subunits, each containing a narrow hydrophobic pore that conducts ammonia. As mentioned earlier, ammonia is a gas at room temperature, but in aqueous solution, it exists predominantly as Am ion (NH_4^+). Questions arise concerning the translocation pathway for ammonia, namely, how a positively charged Am ion NH_4^+ is converted to neutral ammonia, translocates across the hydrophobic channel, and then is reconverted back to NH_4^+ at the other side of the membrane. As reported by Khademi et al.,[12] there exist two vestibules at the top and bottom of the ammonia channel (see Figure 1). It was hypothesized[12] that a wider vestibule site at the periplasmic side of the membrane can recruit NH_4^+ and a narrower 20 Å long hydrophobic channel midway through the membrane can lower the dissociation

† Part of the special issue "William Hase Festschrift".

* To whom correspondence should be addressed. Tel: 419-530-1513. Fax: 419-530-4033. E-mail: xhu@utoledo.edu.

10.1021/jp054261c CCC: $33.50
Published on Web 11/24/2005

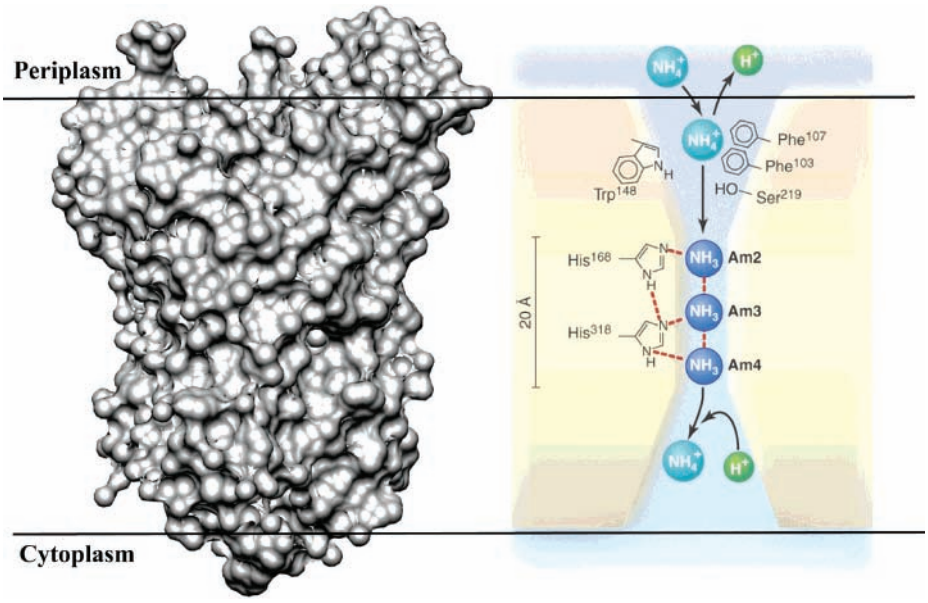

Figure 1. Model of the Am channel based on the 1.35 Å resolution X-ray crystal structure of AmtB from *Escherichia coli* (PDB accession number: 1U7G).[12] Left: Surface representation of the Am channel. Right: A putative mechanism for ammonia translocation according to ref 12 (figure adapted from ref 13).[13] The amino acid residues that line the pore of the outer vestibule (Trp148, Phe107, Phe103, and Ser219) stabilize NH_4^+ (Am1). Midway through the membrane, the channel narrows over a 20 Å span. Here, two pore-lining residues, His168 and His318, stabilize three NH_3 molecules (Am2, Am3, and Am4) through hydrogen bonding (red dashed lines). The molecules return to equilibrium as NH_4^+ in the inner vestibule.

constant of NH_4^+ to facilitate the formation of NH_3, which is then stabilized by interactions with two conserved histidine side chains inside the channel. In a second vestibule at the cytoplasmic end of the channel, the NH_3 returns to equilibrium as NH_4^+. A key assumption for the hypothesized translocation mechanism is that the constellation of aromatic residues in the extracellular vestibule binds Am ions from solution, most likely via cation$-\pi$ interactions.[15,16] A primary goal of this work is to quantify the strengths and analyze the molecular determinants of these cation$-\pi$ interactions.

In addition, it is well-established that the Am transport channel can conduct both Am and MA.[12,17] Competition assays demonstrated that dimethylammonium depresses uptake of MA, but trimethylammonium and tetramethylammonium (TMA) were not inhibitory.[17] Adopting the naming convention in ref 12, ammonium and methylammonium will be denoted Am and MA, respectively, hereafter. TMA refers to tetramethylammonium. Methylation of Am alters its size, hydrophobicity, and hydrogen-bonding capacity. A second goal of this work is to address how the extent of methylation of Am affects its binding affinity with the AmtB channel. In particular, we seek to determine why TMA is not inhibitory to the conduction of Am and MA in the channel.

To achieve the above objectives, we have undertaken two major projects of theoretical studies. In the first project, we have chosen the crystal structures of the Am−AmtB complex and the MA−AmtB complex, as reported by Khademi et al.,[12] for investigation of the molecular determinants of ligand binding. Intermolecular interaction energies between AM (or MA) and its binding pocket in a ligand−protein complex were quantified by means of high level ab initio electronic structure calculations based on the crystal structures of ligand-bound protein complexes.[12] Subsequently, the energetic contribution of each residue in the binding pocket to ligand binding was further analyzed in a pairwise manner so that critical residues for ligand binding and the physical nature of molecular recognition between ligand and protein can be unraveled. In the second project, geometries of the ligand−protein complexes were optimized by means of the hybrid quantum mechanics/molecular mechanics (QM/MM) approach. The QM/MM scheme takes advantage of the best of two worlds: the accuracy of quantum mechanics and the efficiency of molecular mechanics. It was applied to optimize the entire structure of the MA−AmtB complex and the TMA−AmtB complex, respectively. The optimized complex structures were analyzed structurally and energetically to determine the effect of Am methylation. As detailed below, the optimized structure of the TMA−AmtB complex provided, for the first time, a molecular level explanation of why TMA is not inhibitory to translation of Am and MA in the ammonia transport proteins. Clarification of the mechanism with which the Am and MA interact with the AmtB channel protein will generate valuable insight into the rational drug design in targeting the Amts.

The remainder of the article is organized as follows. Detailed implementation of the QM/MM scheme for geometry optimization of the ligand−protein complex, along with a brief description of the supramolecular approach for interaction energy calculation, is given in section II. Section III presents results of intermolecular interaction strengths for ligand binding in the Am−AmtB complex and the MA−AmtB complex, as well as a structural and energetic analysis of the optimized TMA−AmtB complex in comparison with the MA−AmtB complex. A brief summary is given in section IV.

II. Methods

Intermolecular Interaction Energies. The intermolecular interaction energies between ligands and their surrounding residues were calculated by ab initio electronic structure calculations at the MP2/6-311+G** level with the frozen core by means of the supermolecular approach. In the supermolecular approach, the energy of interaction between molecules A and B is defined as the difference between the energy of the interacting dimer E_{AB} and the energies of the monomers E_A and E_B

$$\Delta E = E_{AB} - E_A - E_B$$

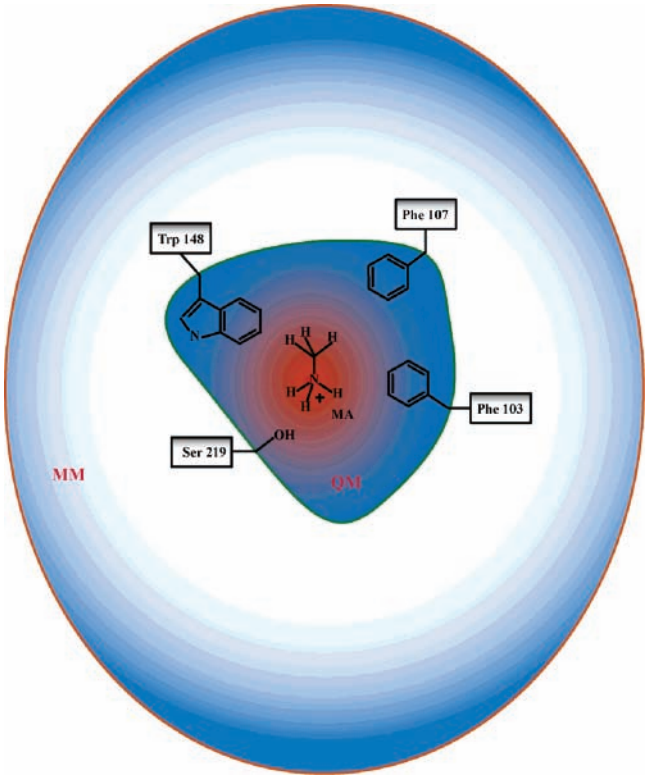

Figure 2. Geometry optimization scheme of MA in its binding pocket of the Am channel protein AmtB. The QM layer (encircled within the green line) contains MA and its direct cation−π interaction and hydrogen-bonding partners and was treated at the HF/6-31+G* level of theory. The MM layer is treated by the AMBER force field.

The calculations were carried out using the Gaussian 03 program[18] at the second-order Moller−Plesset Theory (MP2) using the 6-311+G* basis set (MP2/6-311+G*). The basis set superposition error (BSSE) was corrected by the Boys and Bernardi Counter Poise Method.[19]

QM/MM Optimization. The geometries of the complexes of methylated Ams with AmtB (MA−AmtB and TMA−AmtB) were optimized, respectively, with a hybrid QM/MM approach as implemented in Gaussian 03[18] where the multilayered ONIOM scheme[20] was utilized. As depicted in Figure 2, in the case of the MA−AmtB complex, the scheme partitions the system into an active region treated at a QM level of theory and the larger, remaining region treated by an inexpensive MM method. The interaction zone (see Figure 2) was treated at the Hartree−Fock (HF) level with the 6-31+G* basis set; the latter contains the diffuse functions that are localized sufficiently far from the atomic nuclei and thus fill the empty space between two interacting monomers as needed for a proper treatment of intermolecular interactions.[21−25] The MM layer includes the rest of the entire AmtB protein and is described by the AMBER force field.[26] During the QM/MM optimization, α-carbon atoms for certain residues in the MM layer were constrained. Because the primary objective of the QM/MM optimization is to optimize coordinates of atoms in the intermolecular interaction zone, all of the atoms in the QM layer were free to move. For the MM layer, the α-carbon atoms of all residues except for the aromatic binding site for methylated Am were fixed. The ligand-binding pocket consists of residues with one or more atoms within 4.5 Å of methylated Am, which are Phe103, Phe107, Trp148, and Ser219. The rationale for constraining the α-carbon atoms of these residues was to maintain the overall structural integrity as determined by X-ray crystallography and at the same time allow all side chain atoms to adjust (optimize) their intermolecular positions with respect to the ligand according to the laws of quantum mechanics.

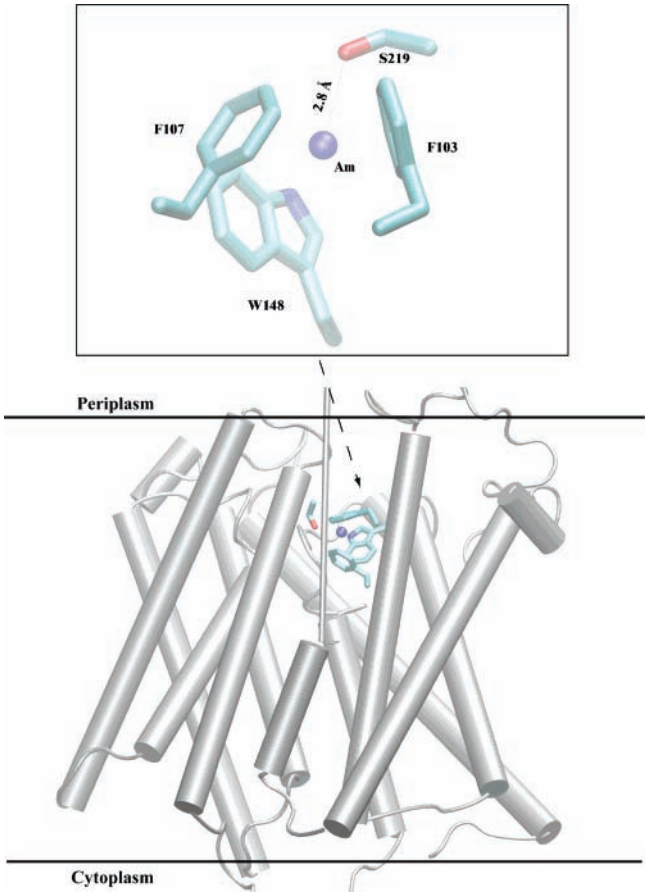

Figure 3. Am ion binding pocket in the outer vestibule of the Am channel AmtB based on its 1.35 Å resolution X-ray crystal structure.[12] Top: Details of the MA ion-binding pocket (H atoms are omitted). The MA ion forms intermolecular interactions with three aromatic residues Trp148, Phe107, Phe103 (via cation−π interactions) and Ser219 (via hydrogen bonding). Bottom: Location of the Am ion-binding pocket in the outer vestibule of AmtB. For clarity, the helix located in front of the binding pocket is shown in a thinner representation to expose the positions of ligands. This plot is generated with the program VMD.[27]

III. Results and Discussion

Intermolecular Interactions between Am (or MA) and AmtB. Intermolecular interaction energies between the Am ion and its binding pocket were calculated by means of the supermolecular approach at the MP2/6-311+G* level based on the 1.35 Å resolution crystal structure of the Am−AmtB complex (PDB accession number 1U7G).[12] As depicted in Figure 3, the binding pocket is defined by any residues with one or more atoms within 4.5 Å of the ligand Am, which includes residues Phe103, Phe107, Trp148, and Ser219. The coordinates of nonhydrogen atoms in Am and its interacting residues in the binding pocket were directly extracted from the X-ray crystal structures. The positions of all hydrogen atoms are placed by ab initio geometry optimization at the HF/6-31G* level with all of the nonhydrogen atom positions fixed.

Likewise, the intermolecular interaction energies between the MA ion and its binding pocket were calculated based on the 1.85 Å resolution crystal structure of the MA−AmtB complex (PDB accession number 1U7C).[12]

Table 1 lists the intermolecular interaction energies between Am (or MA) and its binding pocket at both the HF and the

TABLE 1: Intermolecular Interaction Energies in the Ligand−AmtB Complexes

intermolecular pair	ΔE_{HF} (kcal/mol)[a]	ΔE_{MP2} (kcal/mol)[b]
AM- - -pocket[c]	−39.03	−43.19
MA- - -pocket[c]	−25.61	−35.61

[a] ΔE_{HF} represents interaction energies at the HF/6-311+G* level of theory after BSSE correction. [b] ΔE_{MP2} stands for interaction energies at the MP2/6-311+G* level of theory after BSSE correction. [c] The binding pocket of Am (or MA) includes Phe103, Phe107, Trp148, and Ser219 (see Figure 3).

TABLE 2: Pairwise Intermolecular Interaction Energies in the Ligand−AmtB Complexes

intermolecular pair	ΔE_{HF} (kcal/mol)[a]	ΔE_{MP2} (kcal/mol)[b]
	AM- - -pocket[c]	
AM- - -F103	−2.07	−2.58
AM- - -F107	−10.01	−10.93
AM- - -W148	−15.95	−17.37
AM- - -S219	−18.49	−18.78
	MA- - -pocket[c]	
MA- - -F103	−1.37	−2.88
MA- - -F107	−8.26	−12.72
MA - - -W148	−11.77	−14.51
MA - - - S219	−10.41	−11.13
	TMA- - -pocket[d]	
TMA- - -F103	−0.09	−1.37
TMA- - -F107	−2.34	−2.82
TMA - - -W148	−7.28	−11.47

[a] ΔE_{HF} represents interaction energies at the HF/6-311+G* level of theory after BSSE correction. [b] ΔE_{MP2} stands for interaction energies at the MP2/6-311+G* level of theory after BSSE correction. [c] For Am and MA, coordinates are taken from the crystal structure of the ligand-bound protein complexes.[12] [d] For TMA, the QM/MM optimized structure of the TMA−AmtB complex (see text) is used.

MP2 level of theory. The negative sign represents attractive interactions. The BSSE-corrected MP2/6-311+G* intermolecular interaction energies for the Am−AmtB complex and the MA−AmtB complex are −43.19 and −35.61 kcal/mol, respectively. These are binding energies of substantial magnitude. This is a significant result since it provides a theoretical foundation for the hypothesized role played by the wider vestibule site of AmtB at the periplasmic side of the membrane in acting as a magnet to attract NH_4^+ or MA.[12]

To unravel the underlying physical nature of molecular forces responsible for the calculated strong attractive interactions between Am (or MA) and its binding pocket in the AmtB protein, pairwise interaction energies between Am (or MA) and each residue in its binding pocket were calculated at the same level of theory (MP2/6-311+G*). As shown in Figure 3, the Am ligand is surrounded by the aromatic cage consisting of three aromatic residues Phe103, Phe107, and Trp148. In addition, the hydroxyl group of Ser219 is geometrically positioned favorably for the formation of a hydrogen bond with Am, with a donor−acceptor distance of 2.8 Å. Table 2 lists the pairwise interaction energies between Am and each of the four interacting residues in its binding pocket. The Am- - -Trp148 pair has the strongest interaction strength of −17.37 kcal/mol among the three aromatic residues. The interaction energy for the Am- - -Phe107 pair (−10.93 kcal/mol) is also significant. The Am- - -Phe103 pair displays a relatively weak interaction energy of −2.58 kcal/mol. Adding up the contributions of all three aromatic residues gives rise to a BSSE-corrected MP2/6-311+G* energy of −30.88 kcal/mol for the cation−π interactions between the Am and the aromatic cage. In contrast, the contribution of the Am−Ser219 hydrogen bonding pair is estimated to be −18.78 kcal/mol. These results strongly indicate that the aromatic cage played a crucial role in stabilizing the Am ion at the wider vestibule site of AmtB via cation−π interactions. Also, the hydrogen bonding between the hydroxyl group of Ser219 and the Am has a significant contribution to the favorable binding energetics.

TABLE 3: Comparison of Intermolecular Interaction Energies

intermolecular pair	ΔE_{HF} (kcal/mol)[a]	ΔE_{MP2} (kcal/mol)[b]
	MA[c]	
MA−pocket (crystal)[d]	−25.61	−35.61
	TMA[c]	
TMA−pocket[d]	−17.83	−28.63

[a] ΔE_{HF} represents interaction energies at the HF/6-311+G* level of theory after BSSE correction. [b] ΔE_{MP2} stands for interaction energies at the MP2/6-311+G* level of theory after BSSE correction. [c] For MA, coordinates are taken from the crystal structure of the MA−AmtB complex;[12] for TMA, the QM/MM optimized structure of the TMA−AmtB complex (see text) is used. [d] The binding pocket for MA includes the three aromatic residues Phe103, Phe107, Trp148, and Ser219. The binding pocket of TMA includes Met13, His100, Phe103, Phe107, Gln104, Trp148, Gly218, and Ala220.

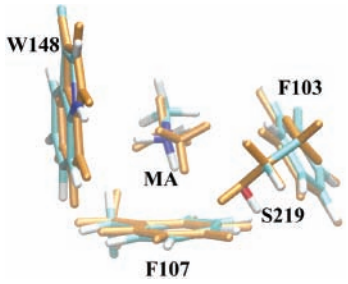

Figure 4. Comparison of the optimized MA−AmtB complex with the crystal structure of the MA−AmtB complex. Superposition of the binding pocket of MA in the optimized structure of the MA−AmtB complex onto the crystal structure of the MA−AmtB complex. All components of the crystal structure of the MA−AmtB complex are shown in orange while those of the optimized MA−AmtB complex are color coded as follows: C, cyan; H, white; and O, red.

It should be pointed out that the gas phase interaction energies as calculated above do not represent a complete picture of ligand−protein association in a cellular environment. To properly evaluate the intermolecular interactions in a biological system, it is necessary to consider solute−solvent interactions. Both the ligand (AM or MM) and the protein (AmtB) are solvated before complex formation. They both lose part of their solvation shell upon binding, which incurs an energy cost commonly referred to as desolvation energy. Past research has indicated that it was necessary to take into consideration the desolvation energies when dealing with cation−π interactions or hydrogen bonds involving positively charged donors.[28,29] How inclusion of desolvation energies affects the intermolecular interaction energies in our systems is an important subject that merits further investigation.

The binding environment of MA in the MA−AmtB complex is very similar to that of Am in the Am−AmtB complex. As a matter of fact, the protein backbones of the two complexes are nearly superimposable (data not shown), and the nitrogen atom of MA in the crystal structure of the MA−AmtB complex is shifted by 0.59 Å against the central nitrogen atom of Am when the protein backbones of the two protein complexes are superimposed. Also, the hydroxyl group of Ser219 has a favorable distance (3.1 Å) for the formation of a hydrogen bond with MA.[12] As detailed in Table 3, pairwise interaction energies

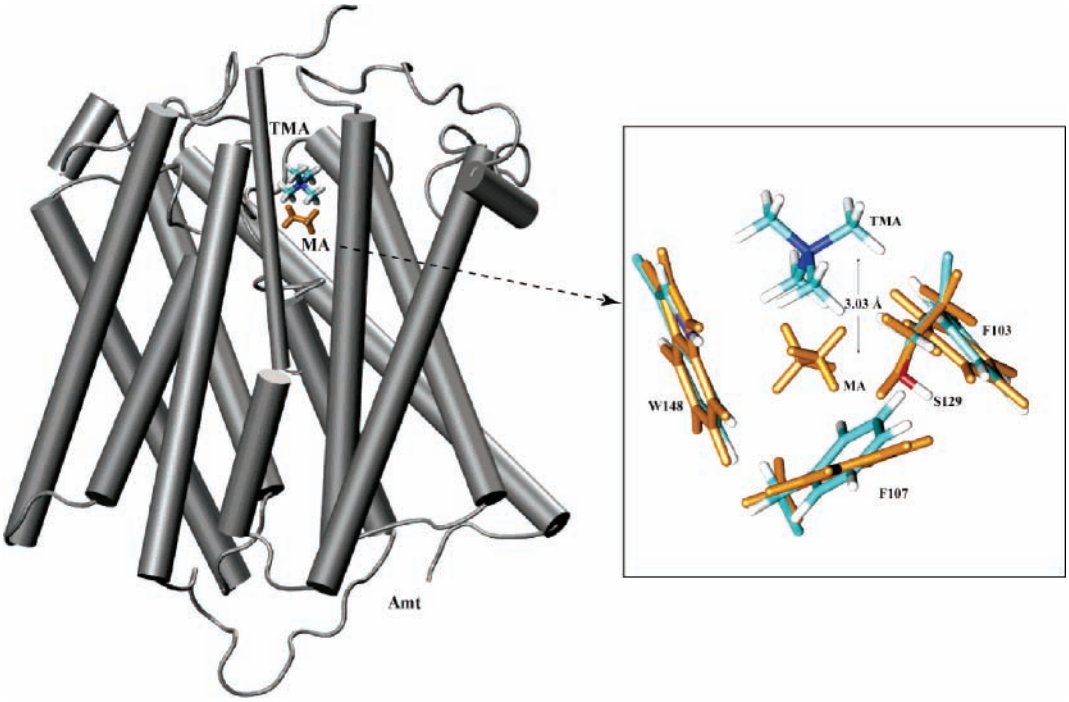

Figure 5. Comparison of the optimized TMA−AmtB complex with the crystal structure of the MA−AmtB complex. Left: superposition of the whole structure of the optimized TMA−AmtB complex onto the crystal structure of the MA−AmtB complex. (For clarity, the helix located in front of the binding pocket is shown in a thinner representation to expose the positions of ligands.) Right: amplified view of the binding pocket alignment. All components of the crystal structure of the MA−AmtB complex are shown in orange while those of the optimized TMA−AmtB complex are color coded as follows: C, cyan; H, white; and O, red.

between MA and its binding pocket in the MA−AmtB complex display a qualitatively similar pattern as those in the Am−AmtB complex.

It is worth noting that comparison of MP2 and HF interaction energies in Table 1 shows a significant amount of correlation correction energies (∼4−10 kcal/mol), which suggests that dispersion energies contribute substantially to the intermolecular interactions between the Am (methylated Am) and the AmtB protein.[24] This further underscores the point that we made earlier about the necessity of including correlation correction when dealing with weakly bonded complexes.[24,25,30]

Structure Optimization of the MA−AmtB Complex and the TMA−AmtB Complex. Geometry optimization for the MA−AmtB complex was carried out with the QM/MM scheme (see Figure 2 above) using the crystal structure of the MA−AmtB complex as the initial configuration. Two structural waters in the immediate geometric proximity of the MA ion form hydrogen bonds with MA and are included as part of the system for geometry optimization. Overall, the optimized structure of the MA−AmtB complex is nearly superimposable with the X-ray crystallography structure of the MA−AmtB complex. Figure 4 displays the superposition of the binding pocket of MA in the optimized structure of the AmtB−MA complex onto the crystal structure of the AmtB−MA complex. The position of MA in the optimized complex is nearly the same as that in the crystal structure. This strongly indicates that the position occupied by MA in the crystal structure of the AmtB−MA complex is energetically favorable.

For comparison, the structure of the TMA−AmtB complex is derived from a similar QM/MM optimization protocol. Because there is no X-ray crystal structure available for the TMA−AmtB complex, the crystal structure of the MA−AmtB complex is employed instead. Computer visualization of the MA−AmtB complex shows that the MA binding pocket has ample space to accommodate TMA spatially. Plus, analyses done by others and us have found that crystal structures with and without Am or MA are identical. Thus, it is a reasonable assumption that binding of TMA to AmtB will not cause a major structural change in the AmtB protein. Under this assumption, the MA molecule in the crystal structure of the MA−AmtB complex[12] (PDB accession number 1U7C) was replaced by the TMA molecule to generate an initial configuration of the TMA−AmtB complex; the latter was then optimized with the QM/MM scheme (see Methods). The optimized structure of the TMA−AmtB complex is superimposed onto the crystal structure of the MA−AmtB complex. Overall, there is no major structural change in the AmtB protein. However, as shown in Figure 5, the optimized position of TMA shifted 3.03 Å against the original MA position in the MA−AmtB crystal structure.

Furthermore, the interaction energies between TMA and its binding pocket in the optimized TMA−AmtB complex were calculated at the MP2/6-311+G* level. The binding pocket of TMA in the complex includes residues Met13, His100, Phe103, Phe107, Gln104, Trp148, Gly218, and Ala220. Listed in Table 3 are intermolecular interaction energies between TMA and its binding pocket in the optimized structure at both the HF/6-311+G* and the MP2/6-311+G* levels of theory. The MP2/6-311+G* calculations resulted in an interaction energy of −28.63 kcal/mol for the interactions of TMA with the entire pocket. The contribution of the aromatic cage to the overall stabilization energy is also analyzed. As listed in Table 2, the interaction energy of TMA with the aromatic cage is −15.66 kcal/mol, which is significantly less than that of MA with the same aromatic cage (see Table 2 and above).

The fact that the optimized position of TMA shifted 3.03 Å against the original MA position in the MA−AmtB crystal structure is in good accord with the experimental observation that TMA is not inhibitory to conducting Am and MA in the Amt channel. It is a strong indication that the position occupied by MA in the MA−AmtB complex is not energetically favorable

for TMA. Therefore, binding of TMA to the AmtB protein does not competitively inhibit binding of MA. This can be attributed in part to the bulky volume of the TMA; the latter acts as the primary barrier for the formation of closer contact deep in the pocket. Also, a lack of hydrogen-bonding capacity of TMA with the Ser219 residue may be responsible for the upward move of TMA in the binding pocket. Judging from the favorable intermolecular interaction energy, the upshifted TMA can still interact with the aromatic cage. However, as shown in Table 2, Trp148 is found to be the only aromatic residue in the cage that is positioned to have a strong cation$-\pi$ interaction with TMA.

The optimized geometry for the MA−AmtB complex also provided us with an opportunity to investigate the effect of geometry optimization of protein−ligand complex on the calculated intermolecular interaction energies between a ligand and its binding protein. Using coordinates from the optimized MA−AmtB complex, the supermolecular approach (see above) resulted in an interaction energy of −41.42 kcal/mol at the MP2/6-311+G* level between MA and its binding pocket; the latter consists of the same residues (i.e., Phe103, Phe107, Trp148, and Ser219) as in the case of the original X-ray crystal structure. For comparison, the calculated MA binding energy at the MP2/6-311+G* level is −35.61 kcal/mol when the original X-ray crystal structure is employed (see Table 1). As expected, the optimized complex structure gives rise to a stronger intermolecular interaction energy. In light of the fact that using coordinates directly taken from X-ray crystal structures for calculating interaction energies of biomolecular systems has long been a general practice in theoretical studies,[22,25,30] it is worth noting here the importance (and necessity) of optimizing the X-ray crystal structure of the protein−ligand complex for quantum mechanical calculations. The reason is 2-fold. On one hand, the energy of the system depends strongly on the positions of the atoms, which means that the results of quantum mechanical analysis are sensitive to the relative positions of interacting molecules. On the other hand, there is a certain degree of uncertainty associated with the atomic coordinates as determined by X-ray crystallography due to the technical limitation of the method itself.[31]

This work represents a timely undertaking for studying the molecular determinants of binding Am ion in the ammonia transport protein AmtB. The substantial strengths of intermolecular interactions as calculated above provide the theoretical support for the hypothesis that the aromatic residues lining the pore of the outer vestibule (Phe103, Phe107, and Trp148) in AmtB act as a magnet to attract NH_4^+ or MA by cation$-\pi$ interactions. Indeed, a cation such as NH_4^+ or MA within the geometric proximity of π-electron cloud of the aromatic residues can experience strong attractive interactions. A wealth of information has been accumulated displaying the importance of such cation$-\pi$ interactions in the formation of biomolecular systems.[16,32,33] The magnitudes of cation$-\pi$ interactions calculated in this study are consistent with results of other biological systems,[16,28,34] as well as results of theoretical models of (methylated)ammonium ions interacting with aromatic rings.[35]

Moreover, the impact of this research will go far beyond an understanding of molecular recognition of Am (and methylated Am) ion in proteins. Molecular recognition is at the center of biological function of proteins, and a profound understanding of the underlying nonbonded interactions is required to intervene in a rational way in biological processes. As stated earlier, Am channel proteins play an important role in all forms of living organisms. Elimination of many therapeutic drugs is associated with their interactions with channel proteins, so knowledge of these interactions may be useful in understanding drug actions of a broad range of pharmaceuticals.

IV. Conclusions

The transport of Am across the cell membrane represents an important biological process in all living organisms. The mechanisms for Am translocation were analyzed by computer simulations based on first principles. QM/MM optimizations and high level quantum mechanism calculations have been performed to study the interactions between differentially methylated Am with the ammonia transporter AmtB. Two major conclusions can be drawn from our studies.

Intermolecular interaction energies between the differentially methylated Am and the Am channel protein AmtB were calculated by means of the supermolecular approach at the MP2/6-311+G* level based on the high-resolution crystal structures of ligand-bound protein complexes. The BSSE-corrected MP2/6-311+G* intermolecular interaction energies for the Am−AmtB complex and the MA−AmtB complex are −43.19 and −35.61 kcal/mol, respectively. These are binding energies of substantial magnitude. Our analysis attributes this strong stabilization energy to the aromatic cage formed by three aromatic residues Phe103, Phe107, and Trp148. The molecular basis of those intermolecular interactions arises from cation$-\pi$ interactions between the positively charged methylated Am and the aromatic residues and CH$-\pi$ interactions between the methyl group(s) and the aromatic residues. This is a significant result since it provides a theoretical foundation for the hypothesized role played by the wider vestibule site of AmtB at the periplasmic side of the membrane in acting as a magnet to attract NH_4^+ or MA.[12] Indeed, the wider vestibule site of AmtB at the periplasmic side of the membrane can act as an aromatic magnet to attract NH_4^+ or MA via cation$-\pi$ interactions. In addition, the hydrogen bonding between the hydroxyl group of Ser219 and the MA has a significant contribution to the favorable binding energetics.

The advanced QM/MM scheme was applied to optimize the structures of methylated Am with the AmtB channel (the MA−AmtB complex and the TMA−AmtB complex). The optimized complex structures were analyzed structurally and energetically to determine the effect of Am methylation. The QM/MM simulations demonstrated that TMA is not able to form as deep a binding to the aromatic cage of the channel protein AmtB as MA. More importantly, our analysis indicated that the optimized position of TMA shifted 3.03 Å in the aromatic cage against the original MA position in the MA−AmtB crystal structure. This can be attributed in part to the bulky volume of the TMA and to a large extent to a lack of hydrogen bonding capacity of TMA with the Ser219 residue that is deep in the binding pocket. This result provides molecular level insights into mechanisms underpinning the experimental observation that TMA is not inhibitory to conducting Am and MA in the Amt channel.[17]

Acknowledgment. This paper is dedicated to William L. Hase in honor of his 60th birthday. We thank him for his dedicated mentorship over the years. We are pleased to acknowledge the Ohio Supercomputer Center for a generous allocation of supercomputer time.

References and Notes

(1) Dommelen, A.; De Mot, R.; Vanderleyden, J. *Aust. J. Plant Physiol.* **2001**, *28*, 959−967.

(2) von Wiren, N.; Gazzarrini, S.; Gojon, A.; Frommer, W. B. *Curr. Opin. Plant Biol.* **2000**, *3*, 254−261.

(3) Ninnemann, O.; Jauniaux, J. C.; Frommer, W. B. *EMBO J.* **1994**, *13*, 3464−3471.
(4) Thomas, G. H.; Mullins, J. G. L.; Merrick, M. *Mol. Microbiol.* **2000**, *37*, 331−344.
(5) Finan, T. M. *Nitrogen Fixation: Global Perspectives: Proceedings of the 13th International Congress on Nitrogen Fixation*, Hamilton, Ontario, Canada, July 2−7, 2001; CABI Publ.: Wallingford, Oxon, United Kingdom, New York, 2002.
(6) Knepper, M. A.; Packer, R.; Good, D. W. *Physiol. Rev.* **1989**, *69*, 179−249.
(7) Nakhoul, N. L.; Hamm, L. L. *Pflugers Arch.* **2004**, *447*, 807−812.
(8) van Montfoort, J. E.; Hagenbuch, B.; Groothuis, G. M. M.; Koepsell, H.; Meier, P. J.; Meijer, D. K. F. *Curr. Drug Metab.* **2003**, *4*, 185−211.
(9) Marini, A. M.; Vissers, S.; Urrestarazu, A.; Andre, B. *EMBO J.* **1994**, *13*, 3456−3463.
(10) Weiner, I. D. *Curr. Opin. Nephrol. Hypertens.* **2004**, *13*, 533−540.
(11) Hemker, M. B.; Cheroutre, G.; van Zwieten, R.; Maaskant-van Wijk, P. A.; Roos, D.; Loos, J. A.; van der Schoot, C. E.; von dem Borne, A. *Br. J. Haematol.* **2003**, *122*, 333−340.
(12) Khademi, S.; O'Connell, J.; Remis, J.; Robles-Colmenares, Y.; Miericke, L. J. W.; Stroud, R. M. *Science* **2004**, *305*, 1587−1594.
(13) Knepper, M. A.; Agre, P. *Science* **2004**, *305*, 1573−1574.
(14) Zheng, L.; Kostrewa, D.; Berneche, S.; Winkler, F. K.; Li, X. D. *Proc. Natl. Acad. Sci. U.S.A.* **2004**, *101*, 17090−17095.
(15) Dougherty, D. A. *Science* **1996**, *271*, 163−168.
(16) Ma, J. C.; Dougherty, D. A. *Chem. Rev.* **1997**, *97*, 1303−1324.
(17) Meier-Wagner, J.; Nolden, L.; Jakoby, M.; Siewe, R.; Kramer, R.; Burkovski, A. *Microbiology (Reading, U. K.)* **2001**, *147*, 135−143.
(18) Frisch, M. J.; et al. *Gaussian 03*, Revision B.04; Gaussian, Inc.: Pittsburgh, PA, 2003.
(19) Boys, S. F.; Bernardi, F. *Mol. Phys.* **1970**, *19*, 553−566.
(20) Vreven, T.; Morokuma, K.; Farkas, O.; Schlegel, H. B.; Frisch, M. J. *J. Comput. Chem.* **2003**, *24*, 760−769.
(21) Sponer, J.; Leszczynski, J.; Hobza, P. *J. Biomol. Struct. Dyn.* **1996**, *14*, 117−135.
(22) Sponer, J.; Berger, I.; Spackova, N.; Leszczynski, J.; Hobza, P. *J. Biomol. Struct. Dyn.* **2000**, Sp. Iss. S2, 383−407.
(23) Sponer, J.; Hobza, P. *Collect. Czech. Chem. Commun.* **2003**, *68*, 2231−2282.
(24) Wang, Y. L.; Hu, X. C. *J. Am. Chem. Soc.* **2002**, *124*, 8445−8451.
(25) Mao, L. S.; Wang, Y. L.; Liu, Y. M.; Hu, X. C. *J. Mol. Biol.* **2004**, *336*, 787−807.
(26) Cornell, W. D.; Cieplak, P.; Bayly, C. I.; Gould, I. R.; Merz, K. M.; Ferguson, D. M.; Spellmeyer, D. C.; Fox, T.; Caldwell, J. W.; Kollman, P. A. *J. Am. Chem. Soc.* **1996**, *118*, 2309−2309.
(27) Humphrey, W.; Dalke, A.; Schulten, K. *J. Mol. Graphics* **1996**, *14*, 33−38.
(28) Mao, L. S.; Wang, Y. L.; Liu, Y. M.; Hu, X. C. *J. Am. Chem. Soc.* **2003**, *125*, 14216−14217.
(29) Gallivan, J. P.; Dougherty, D. A. *J. Am. Chem. Soc.* **2000**, *122*, 870−874.
(30) Wang, Y. L.; Mao, L. S.; Hu, X. C. *Biophys. J.* **2004**, *86*, 3097−3111.
(31) Davis, A. M.; Teague, S. J.; Kleywegt, G. J. *Angew. Chem. Int. Ed.* **2003**, *42*, 2718−2736.
(32) Gallivan, J. P.; Dougherty, D. A. *Proc. Natl. Acad. Sci. U.S.A.* **1999**, *96*, 9459−9464.
(33) Minoux, H.; Chipot, C. *J. Am. Chem. Soc.* **1999**, *121*, 10366−10372.
(34) Bartoli, S.; Roelens, S. *J. Am. Chem. Soc.* **2002**, *124*, 8307−8315.
(35) Pullman, A.; Berthier, G.; Savinelli, R. *J. Am. Chem. Soc.* **1998**, *120*, 8553−8554.